JOURNAL OF AVIATION

e-ISSN: 2587-1676 J Aviat 2020; 4(1): 1-14

Research Article DOI : 10.30518/jav 668240

Sequential Quadratic Optimization of Aeroelastic Energy of Twin-Engine Wing System with Curvilinear Fiber Path

Touraj FARSADI[1*], *Davood ASADI*[1]

Adana Alparslan Türkeş Science and Technology University, Adana, Turkey.

ABSTRACT

In the present study, the aeroelastic energy response of a twin-engine composite wing system is optimized based on sequential quadratic programming (SQP) method. The variable stiffness is acquired by constructing laminates of thin wall beam (TWB) with curvilinear fibers having prescribed paths. In order to account the effect of spanwise locations and mass of the engines on the aeroelastic characteristics of TWB, the novel governing equations of motion are obtained using Hamilton's variational principle. The paper aims to exploit desirable fiber paths with improved aeroelastic properties for different twin-engine wing configuration. Ritz based solution methodology is employed to solve the equations with coupled incompressible unsteady aerodynamic model based on Wagner's function. A novel optimization strategy based on the total energy of the aeroelastic system is introduced. The proposed total energy, as a cost function, is minimized in terms of four optimization variables of two engine's locations and wing structure curvilinear fiber angle with two design parameters. The total energy is obtained by integrating responses of kinetic and potential energy in a specific time interval. The minimum total energy is an indication of ideal optimization variables which leads to the optimum flutter performance. Numerical results demonstrate the effectiveness of the optimization variables on the total energy of the aeroelastic system and determine the optimal values of introduced variables in case of minimum total energy and improved aeroelastic characteristics.

Keywords: aeroelastic optimization, sequential quadratic programming, twin engine-wing system, composite thin walled beam, curvilinear fiber path

1. Introduction

In aircraft design, engine positioning is a challenging task that highly affects the aircraft configuration and characteristics. Engine positioning has major consequences on the aircraft's weight, balance, aerodynamics, structural design, vibration, stability, handling quality, accessibility, maintainability and safety. In fact, several parameters must be considered in determining appropriate locations of engines. For instance, inlet requirements and the resulting effect on engine efficiency dominantly influence the location of engine. Another dominant factor affecting the engine location is the aeroelastic considerations. In modern aviation, various aircraft configurations usually have high-aspect-ratio wings

Corresponding Author: Touraj FARSADI tfarsadi@atu.edu.tr
Citation: Farsadi T., Asadi D. (2020). Sequential Quadratic Optimization of Aeroelastic Energy of Twin-EngineWing System with Curvilinear Fiber Path J. Aviat. 4 (1), 1-14.
ORCID: [1] https://orcid.org0000-0003-0772-3992; [2] https://orcid.org/0000-0002-2066-6016
DOI: https://doi.org/10.30518/jav.668240
Received: 31 December 2019 **Accepted:** 4 June 2020 **Published (Online):** 22 June 2020
Copyright © 2020 Journal of Aviation https://javsci.com - http://dergipark.gov.tr/jav

This is an open access article distributed under the terms of the Creative Commons Attiribution 4.0 International Licence

under which the engines are mounted. In fact, wing–engine configuration has attracted aircraft designers since this configuration provide a significant bending relief on the wing, allowing better wing structure design, and therefore leads to thinner wings with less aerodynamic drag. Besides the aforementioned benefit, the mass and thrust of the engine couple with the aerodynamics and structure of the wing and cause substantial effects on the wing structural frequencies and the flutter speed [1]. The aeroelastic stability of a high-aspect-ratio wing subjected to thrust force has been analyzed by Hodges et. al. [2]. The results demonstrated the effects of thrust magnitude and the ratio of wing bending stiffness to torsional stiffness on the aeroelastic instabilities of the wing. Mardanpour et. al. [3, 4] derived the desired spanwise location of engines and investigated the effect of multiple engine placements on the flying wing geometry. They concluded that the flutter speed considerably increases when the engines are located forward of the wing elastic axis. The influence of engine thrust and arbitrarily engine locations on the flutter boundaries of a cantilever beam model were also investigated in [5-7].

In order to have slender and lighter wing structure, advanced composite materials with thin walled beams (TWBs) structure has been developed. Application of TWBs in aircraft wings as a *load carrying part* of the wing and studying their dynamic behavior has been the topic of many researches [8-13]. Librescu [9] thoroughly investigated the theoretical foundations of composite TWBs and derived the necessary relations. The key point in the composite TWBs is that the desired mechanical and aeroelastic behavior of the structure can be achieved by optimizing and tailoring the directional strength and stiffness of the composite material [14-19]. Initially, the curved fibers were used by Gurdal et al. [20] to vary stiffnesses of rectangular composite plates. Later, Gurdal [21] studied the effects of fiber path definitions on in-plane and out-of-plane response characteristics of flat rectangular variable stiffness laminates. The concept of variable stiffness composites with curvilinear fibers were also investigated in several literatures [22, 23] where the optimization of curvilinear fibers was investigated in designing the composite TWB.

The aircraft structure performance is significantly dependent on the part and quality of the advanced composites used in aircraft. However, it is difficult to achieve good designs of the composites in aircraft structure to guarantee requirements for different missions [24]. Therefore, to fully explore the directional properties of curvilinear fiber composites, the designable ability of aero-structure performance, it is necessary to introduce the principle of optimization to the composite structure design [25-27].

This paper extends the author's previous work [28] on aeroelastic behavior of TWB composite wing- single engine system flutter speed instabilities by optimizing the aeroelastic energy of the twin-engine wing system with variable stiffness. In the present study, the curvilinear fiber paths of a high aspect ratio wing modeled as a thin-walled composite wing carrying two powered engines, arbitrarily located along the wing span, are optimized to achieve the minimum aeroelastic energy which leads to maximum flutter performance. In fact, the wing structure initial and final fiber angles as well as two engines spanwise positions have been considered as the optimization variables. The novel equations of motion that account for the effects of engine mass and thrust force on a composite TWB model with variable curvilinear fibers are discussed. A novel optimization strategy based on the total energy of the aeroelastic system is introduced. The proposed total energy, as a cost function, is minimized in terms of four variables of two engine locations and wing structure two curvilinear fiber angle parameters.

The aeroelastic stabilities of the twin-engine wing system are improved by optimizing the composite fiber paths for different spanwise locations of engines. The governing equations of motion of the twin-engine wing system are obtained utilizing the Hamilton's principle along with a coupled incompressible unsteady aerodynamic model based on Wagner's function. Variable stiffness is acquired by constructing laminates of the walls of the TWB with curvilinear fibers having prescribed paths. Aeroelastic response of the composite wing is performed by means of a Ritz based solution methodology. Asymmetric layup configuration accounts for flapwise bending-torsion coupling which is utilized in load alleviation.

2. Structural Model and Kinematic Relations

As shown in Figure 1, thin walled beam (TWB) studied in this paper is composed of a single cell with straight edges according to Librescu beam theory. The structural model considered is similar to the model developed in Refs. [10, 13, 28] in linear form. For a detailed description of the original structural model, the reader is referred to the

aforementioned references. The TWB model has a length of L, width of l, height of d, and wall thickness of h. As shown in Figure 1, two different coordinate systems are used in mathematical modeling. A Cartesian fixed coordinate system (x, y, z) which is placed at the root, and a local coordinate system (s, n, z). In the local axes, n represents the coordinate axis perpendicular to the tangential coordinate axis s and the origin is at the mid-plane of the wall thickness of the TWB. θ is the angle that fibers make with s axis.

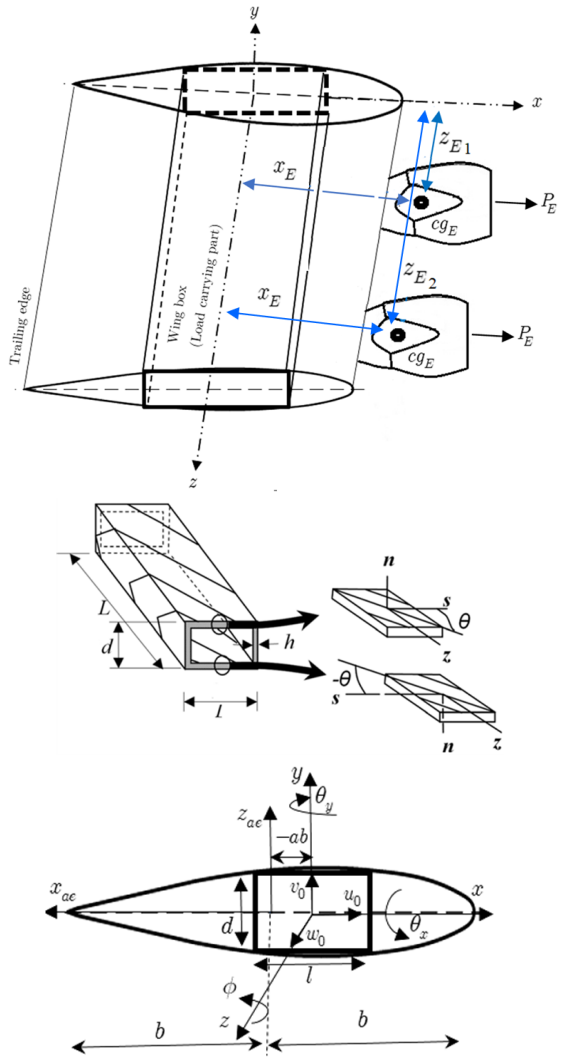

Figure 1. Schematic description of the twin-engine wing system and wing box modelled as TWB and its cross section

As illustrated in Figure 1, in mathematical modeling of the twin-engine wing system, the C.G location of the engines measured from the box shear center and root, is denoted by x_E, z_{E1} and z_{E2} in x and z directions, respectively. Note that the C.G distance in y direction is considered to be very small and negligible.

In deriving the governing equations of motion, basic assumptions in the present study follow those of Ref [9]. The linear displacements of any generic point on the beam (u, v, w) are described in terms of the displacements u_0, v_0, and w_0 rotation angles θ_x, θ_y and ϕ as,

$$\begin{aligned} u &= u_0(z,t) - y\phi(z,t) \\ v &= v_0(z,t) + x\phi(z,t) \\ w &= w_0(z,t) + \left(x + n\frac{dy}{ds}\right)\theta_y(z,t) + \\ &\left(y - n\frac{dx}{ds}\right)\theta_x(z,t) - \left[F_w(s) + na(s)\right]\phi'(z,t) \end{aligned} \tag{1}$$

where,

$$\begin{aligned} \theta_x(z,t) &= \gamma_{yz}(z,t) - v_0'(z,t) \\ \theta_y(z,t) &= \gamma_{xz}(z,t) - u_0'(z,t) \end{aligned} \tag{2}$$

where, u_0, v_0 and w_0 are the translations of the shear center of the thin walled beam in x, y and z directions, and θ_x, θ_y and ϕ are the rotations about x, y and z axes, respectively. Additionally, $\gamma_{yz}(z,t)$, $\gamma_{xz}(z,t)$ represent the transverse shear strains. In Eqs. (1) and (2) prime sign denotes differentiation with respect to the z direction. $F_w(s)$ and $na(s)$ are the primary and secondary warping functions that are given in [10].

Figure 2 illustrates the displacements and the rotations of the TWB cross section with respect to the x, y, z coordinate system established at the root of the TWB.

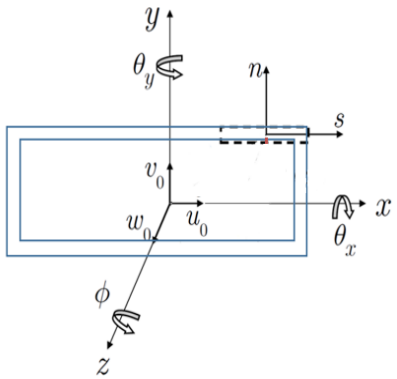

Figure 2. Cross-section of the TWB showing the displacements and rotations

The axial strains associated with the displacement field is,

$$\begin{aligned}
&\varepsilon_{zz}(n,s,z,t) = \varepsilon^0_{zz}(s,z,t) + n\varepsilon^n_{zz}(s,z,t)\\
&\varepsilon^0_{zz}(s,z,t) = w_0'(z,t) + \theta_x'(z,t)y(s) + \theta_y'(z,t)x(s)\\
&\qquad - \phi''(z,t)F_w(s)\\
&\varepsilon^n_{zz}(s,z,t) = \theta_y'(z,t)\frac{dy}{ds} - \theta_x'(z,t)\frac{dx}{ds} - \phi''(z,t)a(s
\end{aligned} \tag{3}$$

The tangential shear strain components can be defined as,

$$\begin{aligned}
&\gamma_{sz}(s,z,t) = \gamma^0_{sz}(s,z,t) + 2\frac{A_C}{S}\phi'(z,t),\\
&\gamma^0_{sz}(s,z,t) = [u_0'(z,t) + \theta_y(z,t)]\frac{dx}{ds} + [v_0'(z,t) + \theta_x(z,t)]\frac{dy}{ds},\\
&\gamma_{nz}(s,z,t) = [u_0'(z,t) + \theta_y(z,t)]\frac{dy}{ds} - [v_0'(z,t) + \theta_x(z,t)]\frac{dx}{ds},
\end{aligned} \tag{4}$$

where $\varepsilon^0_{zz}, \gamma^0_{sz}$ are the normal and shear strain components on the mid-surface of the box beam, respectively. A_C is the area enclosed by the midline contour and S is the contour's perimeter.

2.1. Constitutive relations

The contracted form of relationship between the stresses and strains in a layer can be expressed in terms of the reduced stiffness coefficients $\bar{Q}_{ij}$ of the k^{th} layer of the composite TWB according to Eq. 5.

$$\begin{Bmatrix}\sigma_{ss}\\ \sigma_{zz}\\ \sigma_{nz}\\ \sigma_{sn}\\ \sigma_{sz}\end{Bmatrix}_{(k)} = \begin{bmatrix}\bar{Q}_{11} & \bar{Q}_{12} & 0 & 0 & \bar{Q}_{16}\\ \bar{Q}_{21} & \bar{Q}_{22} & 0 & 0 & \bar{Q}_{26}\\ 0 & 0 & \bar{Q}_{44} & \bar{Q}_{45} & 0\\ 0 & 0 & \bar{Q}_{54} & \bar{Q}_{55} & 0\\ \bar{Q}_{61} & \bar{Q}_{62} & 0 & 0 & \bar{Q}_{66}\end{bmatrix}_{(k)} \begin{Bmatrix}\varepsilon_{ss}\\ \varepsilon_{zz}\\ \gamma_{nz}\\ \gamma_{sn}\\ \gamma_{sz}\end{Bmatrix}_{(k)} \tag{5}$$

The $\bar{Q}_{ij}$ components are used to transform the stiffness coefficients from the principle axes to the material axes. All the above components are defined explicitly in Ref [13]. The 2D first order force and moment resultants of the cross-section of the TWB are defined in terms of the 3D stresses. These terms are derived by integrating the 3D stresses in thickness direction.

3. Twin-Engine Wing System Equations

Governing equations of motion are determined using the Hamilton's principle as below;

$$\delta H = \int_{t_1}^{t_2} \delta \begin{pmatrix} T_w - V_w + W_{ae} + \\ T_e - V_e + W_e \end{pmatrix} dt = 0 \tag{6}$$

where *T*, *V*, and *W* are the total kinetic energy, strain energy, and the work done by external forces. The subscripts w, e and *ae* stand for wing, engine and aerodynamic loads, respectively.

3.1. Kinetic energy of wing-engine system

Variation of the kinetic energy of the wing-beam model is expressed as,

$$\begin{aligned}
&T_w = \frac{1}{2}\int_0^L \oint_C \sum_{k=1}^{m_l}\int_{n_{k-1}}^{n_k} \rho \dot{R}^2 \, dn\, ds\, dz\\
&\delta T_w = \int_0^L \oint_C \sum_{k=1}^{m_l}\int_{n_{k-1}}^{n_k} \rho\, \dot{R}\, \delta\dot{R} \; dn\, ds\, dz =\\
&\qquad \int_0^L \oint_C \sum_{k=1}^{m_l}\int_{n_{k-1}}^{n_k} \rho\, \ddot{R}\, \delta R \; dn\, ds\, dz
\end{aligned} \tag{7}$$

In the above equation, ρ is the average mass density, m_l and n_k are the number of layers and thickness of each layer, respectively. R is the position vector of an arbitrary point on the TWB which is defined as,

$$R = (x+u)\hat{i} + (y+v)\,\hat{j} + (z+w)\hat{k} \tag{8}$$

where u, v, w are displacement components according to Eq. 1.

The kinetic energy due to the engine weight (T_e) is defined as,

$$\begin{aligned}
&T_e = \\
&\begin{bmatrix} M_{E1}(\vec{\dot{\mathbf{R}}}_{e1}.\vec{\dot{\mathbf{R}}}_{e1}) + \\ M_{E1}\begin{pmatrix}\kappa^2_{\phi 1}(\vec{\dot{\phi}}.\vec{\dot{\phi}}) + \kappa^2_{\theta x1}(\vec{\dot{\theta}}_x.\vec{\dot{\theta}}_x) + \\ \kappa^2_{\theta y1}(\vec{\dot{\theta}}_y.\vec{\dot{\theta}}_y)\end{pmatrix}\end{bmatrix}\delta_D(z - z_{E1}) + \\
&\begin{bmatrix} M_{E2}(\vec{\dot{\mathbf{R}}}_{e2}.\vec{\dot{\mathbf{R}}}_{e2}) + \\ M_{E2}\begin{pmatrix}\kappa^2_{\phi 2}(\vec{\dot{\phi}}.\vec{\dot{\phi}}) + \kappa^2_{\theta x2}(\vec{\dot{\theta}}_x.\vec{\dot{\theta}}_x) + \\ \kappa^2_{\theta y2}(\vec{\dot{\theta}}_y.\vec{\dot{\theta}}_y)\end{pmatrix}\end{bmatrix}\delta_D(z - z_{E2})
\end{aligned} \tag{9}$$

$$\begin{aligned}
&\delta T_e = \\
&\begin{bmatrix} M_{E1}(\vec{\ddot{\mathbf{R}}}_{e1}.\delta\vec{\mathbf{R}}_{e1}) + \\ M_{E1}\begin{pmatrix}\kappa^2_{\phi 1}(\vec{\ddot{\phi}}.\delta\phi) + \kappa^2_{\theta x1}(\vec{\ddot{\theta}}_x.\delta\theta_x) + \\ \kappa^2_{\theta y1}(\vec{\ddot{\theta}}_y.\delta\theta_y)\end{pmatrix}\end{bmatrix}\delta_D(z - z_{E1}) +\\
&\begin{bmatrix} M_{E2}(\vec{\ddot{\mathbf{R}}}_{e2}.\delta\vec{\mathbf{R}}_{e2}) + \\ M_{E2}\begin{pmatrix}\kappa^2_{\phi 2}(\vec{\ddot{\phi}}.\delta\phi) + \kappa^2_{\theta x2}(\vec{\ddot{\theta}}_x.\delta\theta_x) + \\ \kappa^2_{\theta y2}(\vec{\ddot{\theta}}_y.\delta\theta_y)\end{pmatrix}\end{bmatrix}\delta_D(z - z_{E2})
\end{aligned}$$

where, $M_E, \kappa_\phi, \kappa_{\theta x}$ and $\kappa_{\theta y}$ are the first and second engine mass and radius of gyration about *z*, *x* and *y* axes respectively. The displacement vector of the engine position ($\vec{\mathbf{R}}_e$) due to the wing deformation is [14],

$$\vec{\mathbf{R}}_e = u_0 i + v_0 j + (w_0 + z_E)k + (x_E + x_e)i_e + y_e j_e + z_e k_e \quad (10)$$

$$\vec{\mathbf{R}}_e = = (u_0 + x_E + x_e - y_e\phi - z_e\theta_y)i + (v_0 + y_e + (x_E + x_e)\phi - z_e\theta_x)j + (w_0 + z_E + z_e + (x_E + x_e)\theta_y + y_e\theta_x)k$$

where,

$$\begin{pmatrix} i_e \\ j_e \\ k_e \end{pmatrix} \approx \begin{bmatrix} 1 & \phi & \theta_y \\ \phi & 1 & \theta_x \\ -\theta_y & -\theta_x & 1 \end{bmatrix} \begin{pmatrix} i \\ j \\ k \end{pmatrix} \quad (11)$$

Finally, the variation of the kinetic energy due to engine weight is obtained as,

$$\delta T_e = -\begin{bmatrix} M_{E1}\ddot{u}_0\delta u_0 + \left(M_{E1}\ddot{v}_0 + M_{E1}x_E\ddot{\phi}\right)\delta v_0 + \left(M_{E1}\ddot{w}_0 + M_{E1}x_E\ddot{\theta}_y\right)\delta w_0 + \left(M_{E1}\kappa_{\theta x1}^2\ddot{\theta}_x\right)\delta\theta_x + \left(M_{E1}x_E\ddot{w}_0 + \left(M_{E1}x_E^2 + M_{E1}\kappa_{\theta y1}^2\right)\ddot{\theta}_y\right)\delta\theta_y + \left(M_{E1}x_E\ddot{v}_0 + \left(M_{E1}x_E^2 + M_{E1}\kappa_{\phi 1}^2\right)\ddot{\phi}\right)\delta\phi \end{bmatrix} \delta_D(z - z_{E1}) \quad (12)$$

$$-\begin{bmatrix} M_{E2}\ddot{u}_0\delta u_0 + \left(M_{E2}\ddot{v}_0 + M_{E2}x_E\ddot{\phi}\right)\delta v_0 + \left(M_{E2}\ddot{w}_0 + M_{E2}x_E\ddot{\theta}_y\right)\delta w_0 + \left(M_{E2}\kappa_{\theta x2}^2\ddot{\theta}_x\right)\delta\theta_x + \left(M_{E2}x_E\ddot{w}_0 + \left(M_{E2}x_E^2 + M_{E2}\kappa_{\theta y2}^2\right)\ddot{\theta}_y\right)\delta\theta_y + \left(M_{E2}x_E\ddot{v}_0 + \left(M_{E2}x_E^2 + M_{E2}\kappa_{\phi 2}^2\right)\ddot{\phi}\right)\delta\phi \end{bmatrix} \delta_D(z - z_{E2})$$

3.2. Potential energy of wing-engine system

The strain energy in terms of the non-zero 3D stress and strain components can be expressed as,

$$V_w = \frac{1}{2}\int_0^L \oint_C \sum_{k=1}^{m_l} \int_{n_{k-1}}^{n_k} \begin{bmatrix} \sigma_{zz}\varepsilon_{zz} + \sigma_{sz}\varepsilon_{sz} + \\ \sigma_{nz}\varepsilon_{nz} \end{bmatrix} dn\, ds\, dz \quad (13)$$

where, the integral is taken over the whole cross-section of the beam and it is assumed that the wing has a length of L. Utilizing the strain displacement relations and taking the integral along the wall thickness and along the contour of the cross-section of the TWB, the strain energy due to the deformation of the wing caused by the internal forces can be expressed as,

$$V_w = \frac{1}{2}\int_0^L \begin{bmatrix} T_z w_0' + Q_x(\theta_y + u_0') + Q_y(\theta_x + v_0') + \\ M_y\theta_y' + M_x\theta_x' + M_z\phi' + B_w\phi'' \end{bmatrix} dz \quad (14)$$

where T_z (axial force), Q_x (chordwise shear force), Q_y (flap-wise shear force), M_x (flap-wise bending moment), M_y (chordwise bending moment), M_z (Saint-Venant twist moment), and B_w (bi-moment or warping torque). One dimensional beam force and moment resultants and their generalized strain counterparts, are related to each other through Eq. (15). Details of force and moment resultants are explicitly defined in our previous study [10, 13].

$$\{F\} = [A]\{D\} \rightarrow \begin{Bmatrix} T_z \\ Q_x \\ Q_y \\ M_y \\ M_x \\ M_z \\ B_\omega \end{Bmatrix} = [a_{ij}]_{7\times 7} \begin{Bmatrix} w_0' \\ (u_0' + \theta_y) \\ (v_0' + \theta_x) \\ \theta_y' \\ \theta_x' \\ \phi' \\ -\phi'' \end{Bmatrix} \quad (15)$$

where F, A, D are the one dimensional beam forces and moment resultants, the resulting stiffness matrix, and generalized strain, respectively. For a single cell thin walled beam, stiffness coefficients a_{ij} are given by the contour integral of the stiffness coefficients as shown in [13]. Potential energy due to engine thrust is given as,

$$V_e = \int_0^{z_{E1}} \left[P_{E1}(z_{E1} - z)\left(u_0'' + \phi v_0''\right)\right] dz + \int_0^{z_{E2}} \left[P_{E2}(z_{E2} - z)\left(u_0'' + \phi v_0''\right)\right] dz \quad (16)$$

where, P_E is the first and second engine thrusts.

The variation of the potential energy due to thrust force is obtained as,

$$\delta V_e = \int_0^{z_{E1}} \begin{bmatrix} P_{E1}(z_{E1}-z)\,\delta u_0'' + \\ P_{E1}(z_{E1}-z)\,\phi\,\delta v_0'' + \\ P_{E1}(z_{E1}-z)\,v_0''\,\delta\phi \end{bmatrix} dz + \int_0^{z_{E2}} \begin{bmatrix} P_{E2}(z_{E2}-z)\,\delta u_0'' + \\ P_{E2}(z_{E2}-z)\,\phi\,\delta v_0'' + \\ P_{E2}(z_{E2}-z)\,v_0''\,\delta\phi \end{bmatrix} dz \quad (17)$$

3.3. External works includes aerodynamic and engine thrust

The work done by the external unsteady aerodynamic force and moment is expressed by,

$$W_{ae} = \int_0^L [L_{ae}(z,t)v_0(z) + M_{ae}(z,t)\phi(z)]\,dz \quad (18)$$

where v_0 and ϕ are plunging and pitching motions, respectively. L_{ae} and M_{ae} denote the unsteady aerodynamic lift force and pitching moment which are defined according to Ref [10] as below:

$$L_{ae}(z,t) = -\pi\rho_\infty b^2(\ddot{v}_0 - U\dot{\phi} + ba\ddot{\phi}) - C_{L_\phi}\rho_\infty Ub\left[\dot{v}_0 - U\phi + ba\dot{\phi} - \frac{b}{2}\left(\frac{C_{L_\phi}}{\pi} - 1\right)\dot{\phi} - \sum_{i=1}^{2}\alpha_i B_i(z,t)\right] \quad (19)$$

$$M_{ae}(z,t) = -\pi\rho_\infty b^3\left[\frac{1}{2}\left(\frac{C_{L_\phi}}{\pi} - 1\right)U\dot{\phi} - Ua\dot{\phi} + a\ddot{v}_0 + b\left(\frac{1}{8} + a^2\right)\ddot{\phi}\right] - C_{L_\phi}\rho_\infty Ub^2\left(\frac{1}{2} + a\right)\left[\dot{v}_0 - U\phi + ba\dot{\phi} - \frac{b}{2}\left(\frac{C_{L_\phi}}{\pi} - 1\right)\dot{\phi} - \sum_{i=1}^{2}\alpha_i B_i(z,t)\right] \quad (20)$$

In the above equations, ρ_∞, b, U are the air density, wing semi-chord length, and free stream speed, respectively. B_i terms have to satisfy Eq. (21). α_i and β_i are known as Wagner's function.

$$\dot{B}_i + \dot{\beta}_i\frac{U}{b}B_i = \dot{w}_{0.75c}(z,t)\ ;\ i = 1,\ 2 \qquad \dot{w}_a(x,y,t) = \ddot{v}_0 - U\dot{\phi} + (ba - x_{ae})\ddot{\phi} \quad (21)$$

The variation of the virtual work due to thrust force is given by,

$$\delta W_e = \int_0^L \hat{\mathrm{P}}_1 . \delta\vec{\mathbf{R}}_{e1}\,\delta_D(z - z_{E1})\,dz + \int_0^L \hat{\mathrm{P}}_2 . \delta\vec{\mathbf{R}}_{e2}\,\delta_D(z - z_{E2})\,dz \quad (22)$$

Where, the thrust force $\hat{\mathrm{P}}$ can be simplified in the inertial coordinate system as,

$$\hat{\mathrm{P}} = P_E\,i + P_E\phi\,j - (P_E\theta_y)\,k \quad (23)$$

Substituting the engine position vector into Eq. (22), the vibrational form of virtual work due to the thrust force can be formulated as,

$$\delta W_e = -\int_0^L \begin{bmatrix} -P_{E1}\,\phi\,\delta v_0 + P_{E1}\,\theta_y\delta w_0 - \\ P_{E1}\,x_E\,\theta_y\,\delta\theta_y - P_{E1}\,x_E\,\phi\,\delta\phi \end{bmatrix}\delta_D(z - z_{E1})\,dz + -\int_0^L \begin{bmatrix} -P_{E2}\,\phi\,\delta v_0 + P_{E2}\,\theta_y\delta w_0 - \\ P_{E2}\,x_E\,\theta_y\,\delta\theta_y - P_{E2}\,x_E\,\phi\,\delta\phi \end{bmatrix}\delta_D(z - z_{E2})\,dz \quad (24)$$

3.4. Aeroelastic governing equation of motion

The wing box is assumed to have the layup configuration of Circumferentially Asymmetric Stiffness (CAS) according to Figure 1. Definition of fiber angles, the stiffness coefficients, coupling stiffness, and the mass/inertia terms of the layup are according to our previous study and the details can be found in Ref. [10, 13].

After quite burdensome manipulation of formulas, the integral form of equation of motion for the TWB composite twin-engine wing system with CAS configuration is obtained as;

$$\int_0^L \begin{pmatrix} f_1(\Delta)\,\delta u_0 + f_2(\Delta)\delta u_0' \\ f_3(\Delta)\,\delta v_0 + f_4(\Delta)\delta v_0' + \\ f_5(\Delta)\,\delta w_0 + f_6(\Delta)\delta w_0' + \\ f_7(\Delta)\,\delta\theta_x + f_8(\Delta)\delta\theta_x' + \\ f_9(\Delta)\,\delta\theta_y + f_{10}(\Delta)\delta\theta_y' + \\ f_{11}(\Delta)\,\delta\phi + f_{12}(\Delta)\delta\phi' + f_{13}(\Delta)\delta\phi'' \end{pmatrix} dz + \int_0^{z_{E1}} (f_{14}(\Delta)\delta v_0'' + f_{15}(\Delta)\delta\phi)\,dz + \int_0^{z_{E2}} (f_{16}(\Delta)\delta v_0'' + f_{17}(\Delta)\delta\phi)\,dz = 0 \quad (25)$$

where Δ is defined as $\Delta \in \{u_0, v_o, w_o, \theta_x, \theta_y, \phi\}$; moreover, the function $f_i\,; i = 1...14$ are given by;

$$f_1(\Delta) = b_1\ddot{u}_0 + M_{E1}\ddot{u}_0\delta_D(z - z_{E1}) + M_{E2}\ddot{u}_0\delta_D(z - z_{E2})$$

$$f_2(\Delta) = a_{22}(\theta_y + u_0') + a_{12}w_0'$$

$$f_3(\Delta) = b_1\ddot{v}_0 + M_{E1}(\ddot{v}_0 + x_E\ddot{\phi})\delta_D(z - z_{E1}) + M_{E2}(\ddot{v}_0 + x_E\ddot{\phi})\delta_D(z - z_{E2}) - P_{E1}\phi\delta_D(z - z_{E1}) - P_{E2}\phi\delta_D(z - z_{E2}) - L_{ae}$$

$$f_4(\Delta) = a_{33}(\theta_x + v_0') - a_{37}\phi''$$

$$f_5(\Delta) = b_1\ddot{w}_0 + M_{E1}(\ddot{w}_0 + x_E\ddot{\theta}_y)\delta_D(z - z_{E1}) + M_{E2}(\ddot{w}_0 + x_E\ddot{\theta}_y)\delta_D(z - z_{E2}) + P_{E1}\theta_y\delta_D(z - z_{E1}) + P_{E2}\theta_y\delta_D(z - z_{E2}) \quad (26)$$

$$f_6(\Delta) = a_{11}w_0' + a_{12}(\theta_y + u_0')$$

$$f_7(\Delta) = a_{33}(v_0' + \theta_x) - a_{37}\phi'' + (b_4 + b_{12})\ddot{\theta}_x + M_{E1}\kappa_{\theta x1}^2\ddot{\theta}_x\delta_D(z - z_{E1}) + M_{E2}\kappa_{\theta x2}^2\ddot{\theta}_x\delta_D(z - z_{E2})$$

$$f_8(\Delta) = a_{55}\theta_x' + a_{56}\phi'$$

$$f_9(\Delta) = a_{12}w_0' + a_{22}(u_0' + \theta_y) + (b_5 + b_{11})\ddot{\theta}_y + M_{E1}(x_E\ddot{w}_0 + (x_E^2 + \kappa_{\theta y1}^2)\ddot{\theta}_y)\delta_D(z - z_{E1}) + M_{E2}(x_E\ddot{w}_0 + (x_E^2 + \kappa_{\theta y2}^2)\ddot{\theta}_y)\delta_D(z - z_{E2}) - P_{E2}x_E\theta_y\delta_D(z - z_{E2})$$

$$f_{10}(\Delta) = a_{44}\theta_y'$$

$$f_{11}(\Delta) = (b_4 + b_{12} + b_5 + b_{11})\ddot{\phi} - P_{E1}x_E\phi\delta_D(z - z_{E1}) - P_{E2}x_E\phi\delta_D(z - z_{E2}) + \begin{pmatrix} M_{E1}x_E\ddot{v}_0 + \\ (M_{E1}x_E^2 + M_{E1}\kappa_{\phi1}^2)\ddot{\phi} \end{pmatrix}\delta_D(z - z_{E1}) + \begin{pmatrix} M_{E2}x_E\ddot{v}_0 + \\ (M_{E2}x_E^2 + M_{E2}\kappa_{\phi2}^2)\ddot{\phi} \end{pmatrix}\delta_D(z - z_{E2}) - M_{ae}$$

$$f_{12}(\Delta) = a_{66}\phi' + a_{56}\theta_x' - b_{10}\ddot{\phi}'$$

$$f_{13}(\Delta) = a_{37}(v_0' + \theta_x) - a_{77}\phi''$$

$$f_{14}(\Delta) = P_{E1}\phi(z_{E1} - z)$$

$$f_{15}(\Delta) = P_{E1}v_0''(z_{E1} - z)$$

$$f_{16}(\Delta) = P_{E2}\phi(z_{E2} - z)$$

$$f_{17}(\Delta) = P_{E2}v_0''(z_{E2} - z)$$

3.5. Description of variable stiffness

Figure 3. illustrates curvilinear fiber configuration $(\theta = \theta(z))$ in which θ denotes the ply-angle measured from the positive *s*-axis toward the positive *z*-coordinate. Fibers start with T_0 angle, varies with *x* and *z* distance and end with T_1 angle. Thus, two design variables are required in each layer to determine the variation of fiber orientation on the surface of the beam.

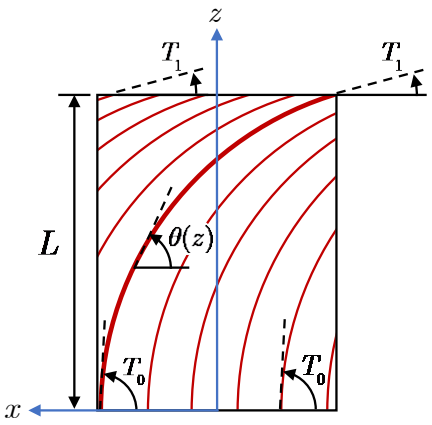

Figure 3. Top view, top spar cap of curvilinear fiber configuration of TWB

As introduced in Ref [18,19], the variation of fiber path for $\theta(z)$ are formulated as,

$$\theta(z) = T_0 + (T_1 - T_0)\left(\frac{z}{L}\right) \quad (27)$$

4. Solution Method

In order to solve the eigenfunctions of TWB with Asymmetric layup, Ritz based solution method utilizing mode shapes of TWB is applied. The mode shapes are used to give the reduced modal matrix *R*, which is derived from the solution of the state space form of TWB equations of motion, for *m* right eigenvectors of the system,

$$R_{6N\times m} = \left[R_{m\times N}^{u^T} \quad R_{m\times N}^{v^T} \quad R_{m\times N}^{w^T} \quad R_{m\times N}^{x^T} \quad R_{m\times N}^{y^T} \quad R_{m\times N}^{\phi^T}\right] \quad (28)$$

Seven trial functions, sufficient for convergence of flutter solutions, are used to meet the boundary conditions of clamped-free wing structure. A reduced order model for six degree of freedom $\Delta \in \{u_0, v_0, w_0, \theta_x, \theta_y, \phi\}$ is then introduced in terms of pertinet trial functions ψ^{Δ} and related reduced modal matrix $\boldsymbol{R}^{\Delta}$ composed of main *m* right eigenvectors of the modal coordinates as,

$$\Delta(z,t) = \psi^{\Delta^T} R^{\Delta} \vartheta(t) \tag{29}$$

Where $\vartheta(t)$ is the generalized modal coordinate vector with dimension of $m \times 1$, $\boldsymbol{R}^{\Delta}$ is the reduced modal matrix with dimension of $N \times m$ composed of dominant m right eigenvectors corresponding to any degrees of freedom Δ, and ψ^{Δ} is the vector of trial functions, with dimension of $N \times 1$, corresponding to any degrees of freedom Δ. The test functions for any degrees of freedom are defined by the premultiplication of the vector of the trial functions ψ^{Δ}. The reduced modal matrix $\boldsymbol{L}^{\Delta^T}$ is composed of dominant m left eigenvectors corresponding to the translational and rotational degrees of freedom, as below,

$$\delta\Delta(z) = L^{\Delta^T} \psi^{\Delta} \tag{30}$$

Modal expansions of the degrees of freedom of the TWB (Eq. (29)) and the variations of the degrees of freedom (Eq. (30)) are substituted into the integral form of the governing equations of motion of Eq. (25). Applying the substitutions results in the following reduced order system of linear equations,

$$M_t \ddot{\vartheta}(t) + C_t \dot{\vartheta}(t) + K_t \vartheta(t) - Z(t) = 0 \tag{31}$$

where $\boldsymbol{M}_t, \boldsymbol{C}_t, \boldsymbol{K}_t$ are the reduced order mass, aerodynamic damping, and stiffness matrices of dimension $m \times m$, respectively, and Z is the reduced order vectors of dimension $m \times 1$ which includes the aerodynamic lag states.

In the resulting reduced order system of equations, if the modal matrices composed of the left $(\boldsymbol{L}^T)$ and the right eigenvectors $(\boldsymbol{R})$ are factored out, reduced order mass, damping and stiffness matrices in Eq. (31) are defined as,

$$\begin{aligned} \boldsymbol{M}_t &= L^T(\boldsymbol{M}_s + \boldsymbol{M}_{ae})R \\ \boldsymbol{C}_t &= L^T \boldsymbol{C}_{ae} R \\ \boldsymbol{K}_t &= L^T(\boldsymbol{K}_s + \boldsymbol{K}_{ae})R \end{aligned} \tag{32}$$

where $\boldsymbol{M}_s$ and $\boldsymbol{K}_s$ are the structural mass, stiffness matrices, and $\boldsymbol{M}_{ae}$,, $\boldsymbol{K}_{ae}$ and $\boldsymbol{C}_{ae}$ are the aerodynamic mass, stiffness, and damping matrices of dimension $6N \times 6N$, respectively. Considering virtual work done by unsteady lift and moment due to aerodynamic lag states, the final form of the aeroelastic system of equations of the CAS configuration composite wing modelled as TWB can be obtained in state space representation as given in Eq. (33).

$$\begin{bmatrix} C_t & M_t & 0 & 0 \\ I & 0 & 0 & 0 \\ D_1 & D_2 & -I & 0 \\ D_1 & D_2 & 0 & -I \end{bmatrix} \frac{d}{dt} \begin{Bmatrix} \vartheta \\ \dot{\vartheta} \\ \hat{B}_1 \\ \hat{B}_2 \end{Bmatrix} + \begin{bmatrix} K_t & 0 & \alpha_1 I & \alpha_1 I \\ 0 & -I & 0 & 0 \\ 0 & 0 & (-\beta_1 U / b)I & 0 \\ 0 & 0 & 0 & (-\beta_2 U / b)I \end{bmatrix} \begin{Bmatrix} \vartheta \\ \dot{\vartheta} \\ \hat{B}_1 \\ \hat{B}_2 \end{Bmatrix} = 0 \tag{33}$$

Eq. (33) is in the form,

$$A\dot{q}(t) + Bq(t) = 0 \tag{34}$$

Where q is the state vector of dimension $4m \times 1$ and $\boldsymbol{A}$ and $\boldsymbol{B}$ are $4m \times 4m$ coefficient matrices defined in Eq. (33). In more compact form, Eq. (34) can be re-written as,

$$\{\dot{q}\} = [\mathbb{R}]\{q\} \tag{35}$$

The solution to Eq. (35) is written as,

$$\{q(t)\} = \{q_0\} e^{\lambda t} \tag{36}$$

where $\{q_0\}$ is an amplitude vector and λ is the eigenvalue, both of which can be complex quantities. Substituting Eq. (36) into Eq. (35), one obtains the eigenvalue problem as given in Eq. (37),

$$[\mathbb{R}] = \lambda \{q_0\} \tag{37}$$

Solution of Eq. (37) yields the eigenvalues λ and the corresponding eigenvectors. Aeroelastic respose of the composite wing modeled as TWB is performed in time domain by the direct integration of Eq. (34) using the Runge-Kutta method for the prescribed initial conditions.

5. Optimization Strategy

The main objective of this research is to enhance the aeroelastic response of the flexible wing engine system by optimizing the wing structure fiber angle orientations and the spanwise locations of engines. This section presents optimization problem formulation including optimization variables, cost functions, and constraints. The optimization problem is actually a nonlinear constraint optimization which is solved applying the Sequential Quadratic Programming (SQP) algorithm.

5.1. Cost functions

In the proposed optimization approach a novel energy based cost function is introduced and the optimization variables are optimized to have the minimum value of cost function. The energy expression is defined based on the aeroelastic response of the twin- engine wing system. In fact, lower values of the system total energy are an indication of more appropriate values of structure fiber angle orientations and the engine's positions respecting the aeroelastic response of wing-engine system during flutter.

The energy cost function is defined based on the total system energy, including the total system strain energy and kinetic energy which are written in matrix form as below;

$$U = \frac{1}{2} q^T K_t \, q \tag{38}$$

$$T = \frac{1}{2} \dot{q}^T M_t \, \dot{q} \tag{39}$$

According to the above system energy terms, the cost function is defined as the integral summation of strain and kinetic energy as below;

$$\mathrm{I}_{CF} = \int_0^t (\frac{1}{2} q^T K_t \, q + \frac{1}{2} \dot{q}^T M_t \, \dot{q}) \, dt \tag{40}$$

Where K_t and M_t are the total structural and aerodynamic stiffness and mass of the twin-engine wing system. I_{CF} is the optimization cost function. The above equation is the system total energy in a specific time interval (0,t). In our optimization procedure an interval of 3 seconds (t=3s) have been considered.

5.2. Optimization variables and constraints

The design variables considered in the optimization procedure in this research includes; the wing structure initial (T_0) and final (T_1) fiber angle orientation, spanwise location of the first engine (z_{E1}) and the second engine (z_{E2}) on the wing. Therefore, the four optimization variables can be expressed as,

$$OptimVars = [T_0 \, , \, T_1 \, , \, z_{E1} \, , \, z_{E2}] \tag{41}$$

All the design variable can continuously vary inside a specific range depending on logical and geometric constraints. Based on the wing span length, which is 14 *m*, the first and second engine location is considered to vary in the interval of (2,7) and (5,13) meters, respectively. The wing structure initial and final fiber angle orientation can vary continuously between zero and -90 degrees. Therefore, all the variables constraints which are the lower and upper bound of variables, can be expressed as below:

$$\begin{aligned} 0 \; &\leq T_0 \; \leq -90 \\ 0 \; &\leq T_1 \; \leq -90 \\ 2 \; &\leq z_{E1} \; \leq 7 \\ 5 \; &\leq z_{E2} \; \leq 13 \end{aligned} \tag{42}$$

5.3. Optimization algorithm

After defining and formulating the optimization variables, constraints, and cost function according to previous section, an optimization algorithm should be implemented to solve the problem. In this research, the optimal values of optimization variables have been derived applying Sequential Quadratic Programming (SQP) which is a numerical optimization algorithm. Sequential Quadratic Programming (SQP) is one of the most successful methods for the numerical solution of constrained nonlinear optimization problems. We consider the nonlinear, constrained optimization problem to minimize the objective function which is the total energy of the system, under 4 inequality constraints. In this research, the *fmincon* function with SQP based optimization algorithm of MATLAB version 2019*b* has been applied to solve the problem on a 16 cores computer of 3.4 GHz processor, and 32 GB memory.

6. Numerical Results

In this section, the above formulation is applied and the numerical results are presented for the aeroelastic stability boundaries of the Asymmetric configuration for TWB composite wing.

To investigate the effect of fiber path function on the aeroelastic characteristics of twin-engine wing system, the most desirable fiber path is calculated for different engine positions on the wing. The goal here is to find the desired fiber path angle to reach the minimum total energy and maximum flutter speed for arbitrary positions of engine.

6.1. Validation of structural and aeroelastic model

In order to validate the structural model of the engine wing system, natural frequencies are compared with those of presented in Ref [14]. Librescu [14] investigated TWB with unidirectional fiber path meaning the same initial and final path angles ($T_0 = T_1$). In his study, wing natural

frequencies under the effect of mass store were explored.

Table 1 represents the natural frequencies of wing-store configuration of Ref [14] and the results of the engine wing configuration (without thrust force) derived in the present paper for different fiber angles. According to Table 1, the results presented in this paper are satisfactorily close to those of Ref [14]. Less than 2 percentage of difference is observed in the first, second, and third natural frequencies in various fiber angles

Table 1 Natural frequencies with under wing store/engine

1st Frequency			2nd Frequency			3rd Frequency		
θ	Ref [14]	Present	θ	Ref [14]	Present	θ	Ref [14]	Present
90°	3.07	3.09	90°	3.65	3.7	90°	14.77	14.86
75°	2	2.04	75°	5.5	5.57	75°	11.9	12.07
60°	1.4	1.44	60°	6.06	6.1	60°	8.87	9.1
45°	1.02	1.05	45°	5.12	5.16	45°	6.25	6.34
30°	0.9	0.92	30°	4.41	4.49	30°	4.94	5.1
15°	0.88	0.9	15°	3.82	3.9	15°	4.87	5.02

6.2. System energy

This section represents the effect of external engine masses on the total energy of the composite TWB. Note that evaluating engine without the propulsion force can be considered as engine out as well as external stores. For each case of engine position, the minimum total energy is optimized for different fiber path angles. In the numerical results, the wing structure is simulated as a uniform rectangular cross-sectional composite beam, characterized in Table 2. Note that $\bar{M}\left(\equiv M_E \Big/ \left(b_1\big|_{\theta=45^0} \times L\right)\right)$ and $\bar{P}\left(\equiv P_E L^2 \Big/ \sqrt{a_{55}\big|_{\theta=45^0} \times a_{66}\big|_{\theta=45^0}}\right)$ in Table 2 are dimensionless parameters of engine mass and thrust force, respectively.

The results of total energy for fiber angle θ = -60º and z_{E2} =7 m (both are fixed) for spanwise variation of the first engine position are investigated in Figure 4 Accordingly, the optimum total energy which leads to maximum flutter speed for the second engine position of 7 m and fiber angles -60º is the first engine position of z_{E1} =3.1 m.

Table 2 Wing material and wing-engine geometric properties

Material properties		Geometrical properties	
E_1	206.8 (GPa)	L,l,d,h	14, 0.757, 0.1, 0.03 (m)
E_2=E_3	5.17 (GPa)	b	0.8 (m)
G_{12}=G_{13}	3.1 (GPa)	M	0.27
G_{23}	2.55 (GPa)	P	13.8
υ	0.25	$\kappa_{\theta x}$, $\kappa_{\theta y}$, κ_{Φ}	0.3,0.6.0.6
ρ	1528 (kg/m^3)		

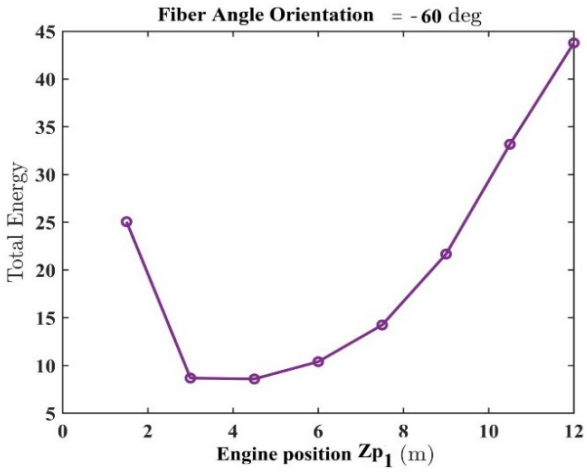

Figure 4. variation of total energy for fiber angle -60º for various first engine positions

In order to illustrate the effect of wing fiber angle on the cost function, the total energy response of twin-engine wing system for straight fiber angles of θ = -45º and -75º have been shown in 2.5 seconds in Figure 5. The total energy is calculated based on the formulation given in Equation (40). Figure 5 is plotted for near flutter speed of 85 m/s with the same position of engines.

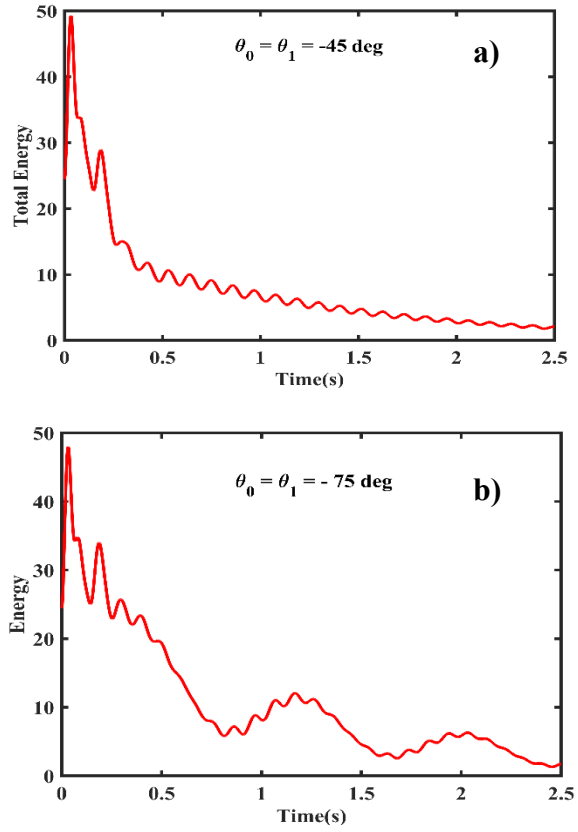

Figure 5. The effect of host structure fiber angle orientation with fixed position of engines of energy response at near flutter speed 85 m/s for angles a) -45º and b) -75º

The analysis results of the optimization depicted in Figure 6 show that the minimum total energy of one-engine wing system with curvilinear fiber path is calculated for [T_0 = -34.28º, T_1 = -40.35º] and engine spanwise location of z_{E1} =2.1 *m*.

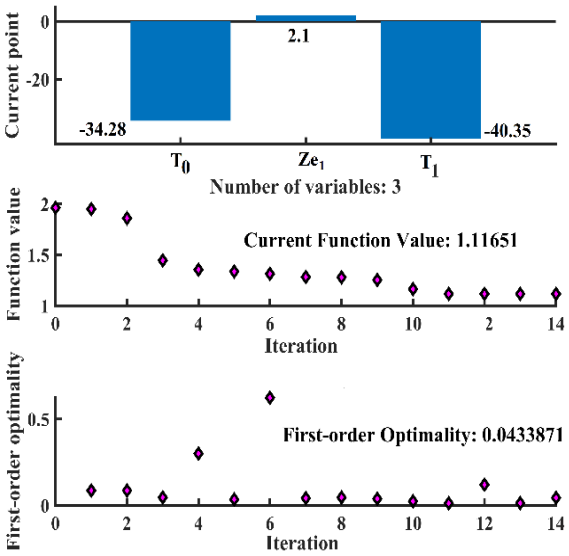

Figure 6. Optimization result, optimal initial and final fiber angle orientation and optimal engine position

By using the SQP algorithm, Figure 7 shows the variation of optimization variables and the number of iterations during the optimizing process for three optimization variables.

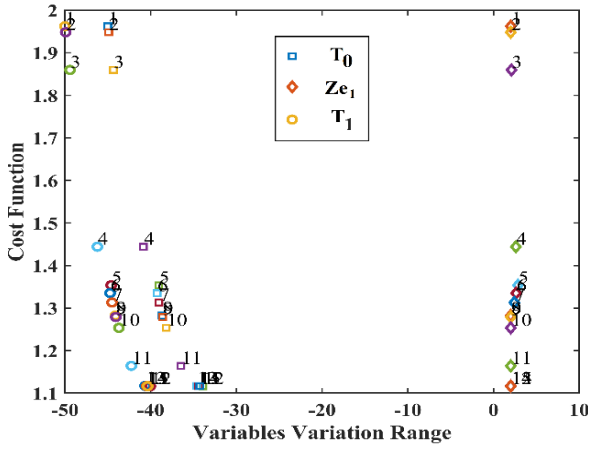

Figure 7. Variation of optimization variables in the optimization iteration, numbers show the number of iterations (14 iterations) in optimization process

As the number of design variables increased in the twin-engine wing system, the optimization can be completed in several minutes. The optimization

results in a minimizing of the total energy of the twin-engine wing system is shown in Figure 8. As a result of the optimization, the minimum total energy with 4 optimization variable is calculated for [T_0 =-41.1º, T_1 =-45.8º] and engines spanwise location of z_{E1} =3.32 m and z_{E2} =7.48 m.

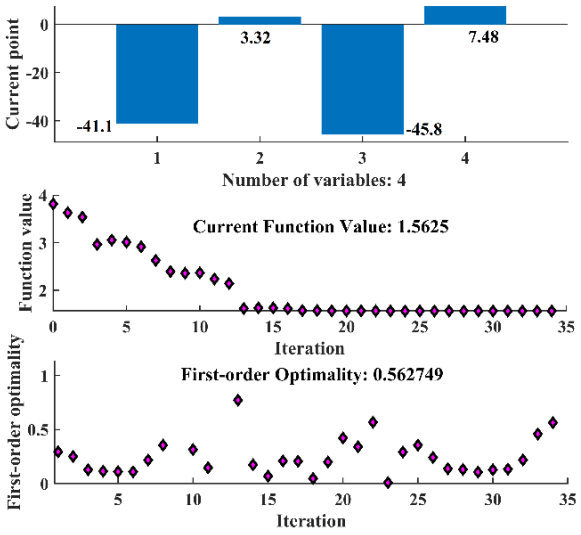

Figure 8. Optimization result, optimal initial and final fiber angle orientation and optimal position of first and second engine

By using the SQP algorithm, Figure 9 shows the second engine position variation and number of iterations during the optimizing process.

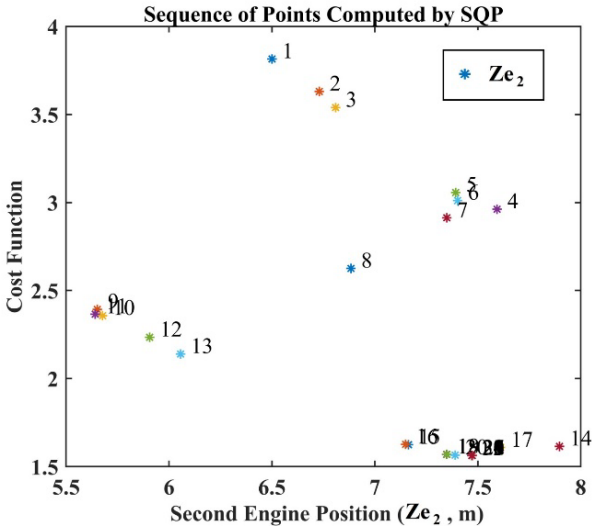

Figure 9. Optimization variable (z_{E2}) in the optimization iteration, numbers show the number of iterations (34 iterations) in optimization process

In examining aeroelastic response in incompressible flight speeds, the effect of the straight and optimum curvilinear fiber layups on the modes response is investigated. Figure 10 shows the computed responses for the flapwise bending and torsion modes for three fiber orientations of θ = −60◦, −75◦ and θ → [T_0 =-41.1º, T_1 =-45.8º]. The flight speed of the present model is considered for U = 85 m/s. The engine positions are considered to be located at optimum positions (Figure (8)) as z_{E1} =3.32 m and z_{E2} =7.48 m along the spanwise. The longest time needed for the damping of the responses is seen for θ = −75◦. However, by changing the ply orientation path to optimum (Figure (8)) curvilinear fiber [T_0 =-41.1º, T_1 =-45.8º] at the same speed, the response amplitude and the response damping time decrease due to the lowest total energy level. This reveals that the directionality property featured by the curvilinear fiber layups can be effectively used to postpone the onset of the flutter instability.

7. Conclusion

In the present study, linear aeroelastic analysis of twin-engine wing system with curvilinear fiber path under the influence of engine is examined using Librescu thin walled beam (TWB) theory. The structural equations of motion are obtained for the asymmetric lay-up composite configuration considering the engine mass and thrust force. The Wagner's unsteady incompressible indicial aerodynamics model is constructed in the time domain by incorporating two aerodynamic lag states. Aeroelastic system of equations for the twin-engine wing system is solved using Ritz method. The novel aspects of this study are derivation of aeroelastic twin-engine wing system equations and application of curvilinear fiber path on aeroelastic performance improvement. Additionally, a novel optimization strategy based on the total energy of the aeroelastic system is introduced. The proposed integral of total energy, as a cost function, is minimized in terms of four optimization variables of two engine locations and wing structure curvilinear fiber angle with two parameters including the initial and final angle orientations. The introduced cost function is optimized with different curvilinear fiber path for various spanwise locations of engine on the wing. For the twin engine TWB wing system, applying curvilinear fiber is seen to be very advantageous on minimizing the cost function and therefore maximizing flutter performance of the wing compared to the unidirectional one.

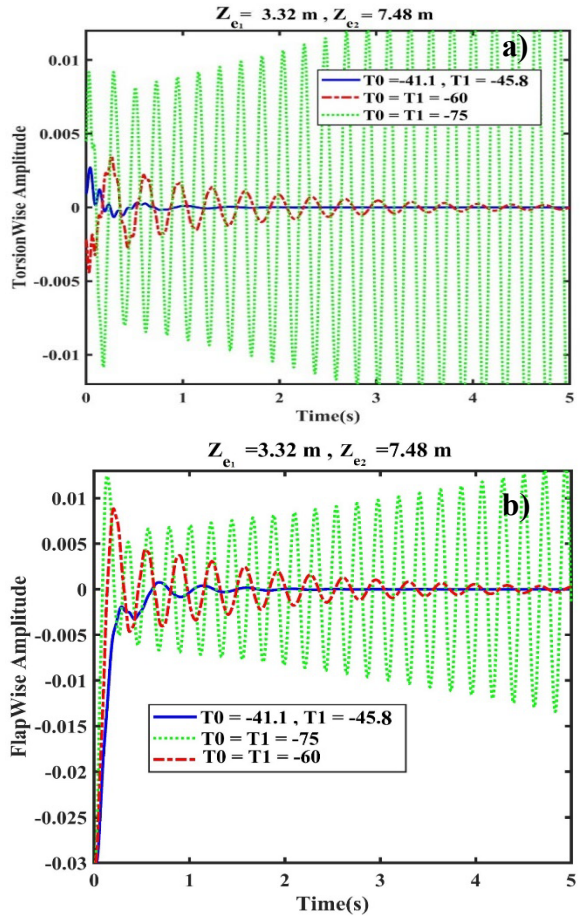

Figure 10. Dynamic aeroelastic a) torsion and b) flapwise bending responses for variations of curvilinear and straight fiber angles

Nomenclature

a = Dimensionless coefficient in offset between mid-chord and box beam shear center

b, l, d, h, L = Half chord, width, height, thickness and length of TWB, respectively

CAS = Circumferentially Asymmetric Stiffness lay-up configuration

C.G = Centre of Gravity

s, n, z = Local coordinate system located at the mid plane of the cross section of TWB

x, y, z = Cartesian fixed coordinate system located at the root of TWB

a_{ij} = Stiffness matrix coefficients

$F_w(s)$, $na(s)$ = Primary warping function, Secondary warping function

L_{ae}, T_{ae} = Unsteady aerodynamic lift and moment

M_E, $\bar{M}$ = Mass of the engine and its dimensionless counterpart

P_E, $\bar{P}$ = Thrust force of the engine and its dimensionless counterpart

T_0, T_1 = Initial and final fiber angles

u_0, v_0, w_0 = Translations of the shear center along x, y, z axes, respectively

x_E, z_E = Engine chordwise and spanwise position, respectively

θ = Fiber angle

λ = Complex values eigenvalue of the aeroelastic system

$\vartheta(t)$ = Generalized modal coordinate

θ_x, θ_y, ϕ = Rotations of the cross section about x, y, z axes, respectively

δ_D = Dirac delta function

ψ^{Δ} = Vector of trial functions

U = Inflow speed

ϕ_W = Wagner's function

$\kappa_{\theta x}, \kappa_{\theta y}, \kappa_{\phi}$ = Radius of Gyration in x, y, z directions

Ethical Approval

Not applicable.

References

[1] Che, Q. L., Han, J., L., and Yun, H., W., "Flutter analysis of wings subjected to engine thrusts," Journal of Vibration Engineering, Vol. 25, No. 2, 2012, pp. 110-116.

[2] Hodges, D., H., Patil, M., J., Chae, S., "Effect of thrust on bending-torsion flutter of wings," Journal of Aircraft, Vol. 39, 2002, p. 371-376.

[3] Mardanpour, P., Hodges, D.H., Neuhart, R., Graybeal, N., "Engine placement effect on nonlinear trim and stability of flying wing aircraft," Journal of Aircraft, 2013, doi:10.2514/1.C031955.

[4] Mardanpour, P., Richards, P.W., Nabipour, O., Hodges, D.H., "Effect of multiple engine placement on aeroelastic trim and stability of flying wing aircraft," In: Proceedings of the 54th AIAA/ASME/ASCE/AHS/ASC Structures,

[5] Mazidi, A., Fazelzadeh, S., A., "The flutter of a swept aircraft wing with a powered-engine," Journal of Aerospace Engineering, Vol. 23, 2010, pp. 243–250.

[6] Fazelzadeh S. A., Azadi M., Azadi E., "Suppression of nonlinear aeroelastic vibration of a wing/store under gust effects using an adaptive-robust controller," Journal of Vibration and Control, Vol. 23, No. 7, 2017, pp. 1206-1217.

[7] Amoozgar, M. R., Irani, S., and Vio, G., A., "Aeroelastic instability of a composite wing with a powered-engine," Journal of Fluids Structures, Vol. 36, 2013, pp. 70–82.

[8] Stodieck, O., Cooper, J., E., Weaver, P., M., and Kealy, P., "Aeroelastic Tailoring of a Representative Wing Box Using Tow-Steered Composites," AIAA Journal, Vol. 55, No. 4, pp. 1425-1439, 2017.

[9] Librescu, L., Song, O., Thin walled composite beam theory and application, USA: Springer, 2006.

[10] Farsadi, T., Rahmanian, M., Kayran, A., "Geometrically nonlinear aeroelastic behavior of pretwisted composite wings modeled as thin walled beams," Journal of Fluids and Structures, Vol. 83, pp. 259-292, 2018.

[11] Farsadi, T., Hasbestan, J., "Calculation of flutter and dynamic behavior of advanced composite swept wings with tapered cross section in unsteady incompressible flow," Mechanics of Advanced Materials and Structures, 2017, doi.org/10.1080/15376494.2017.1387322.

[12] Qin, Z., Librescu, L., "Aeroelastic instability of aircraft wings modeled as anisotropic composite thin-walled beams in incompressible flow," Journal of Fluids and Structures, Vol. 18, No. 1, 2003, 43–61.

[13] Farsadi, T., Sener, O., Kayran, A., "Free vibration analysis of uniform and asymmetric composite pretwisted rotating thin walled beam," In Proceedings of the International Mechanical Engineering Congress and Exposition, Advances in Aerospace Technology, IMECE2017-70531, 3–9 November 2017, Florida, USA.

[14] Librescu, L. and Song, O., "Dynamics of Composite Aircraft Wings Carrying External Stores," AIAA Journal, Vol. 46, No. 3, March 2008.

[15] Gjerek, B., Drazumeric, R., Kosel, F., "Flutter behavior of a flexible airfoil: Multi-parameter experimental study," Aerospace Science and Technology, Vol. 36, 2014, pp. 75–86.

[16] Attaran, A., Majid, D., L., Basri, S., Rafie, A., S., Abdullah, E., J., "Structural optimization of an aeroelastically tailored composite flat plate made of woven fiberglass/epoxy," Aerospace Science and Technology, Vol. 15, 2011, pp. 393–401.

[17] Guo, S., "Aeroelastic optimization of an aerobatic aircraft wing structure," Aerospace Science and Technology, Vol., No.11, 2007, pp. 396–404.

[18] Zamani, Z., Haddadpour, H. and Ghazavi, M., "Curvilinear fiber optimization tools for design thin walled beams," Thin-Walled Structures, Vol. 49, No. 3, 2011, pp. 448-454.

[19] Haddadpour, H., Zamani, Z., "Curvilinear fiber optimization tools for aeroelastic design of composite wings," Journal of Fluids and Structures, Vol. 33, 2012, pp. 180-190.

[20] Gurdal, Z., and Olmedo, R., "In-plane response of laminates with spatially varying fiber orientations: variable stiffness concept," AIAA Journal, Vol. 31, No. 4, 1993.

[21] Gürdal, Z., Tatting, B.,F., and Wu, C., K., "Variable stiffness composite panels: Effects of stiffness variation on the in-plane and buckling response," Composites Part A: Applied Science and Manufacturing, Vol. 39, 2008, pp. 911-922.

[22] Akhavan, H., Ribeiro, P., "Natural modes of vibration of variable stiffness composite laminates with curvilinear fibers," Composite Structures, Vol. 93, No. 11, 2011, pp. 3040-3047.

[23] Gunay, M., G., Timarci, T., "Static analysis of thin-walled laminated composite closed-section beams with variable stiffness," Composite Structures, Vol. 182, 2017, pp. 67-78.

[24] Zhang, Y., Xiong, F., & Yang, S., "Numerical simulation for composite wing structure design optimization of a minitype unmanned aerial vehicle". The Open Mechanical Engineering Journal, 5(1), 2011.

[25] Chang N., Yang W., Wang J., and Wang W., "Design optimization of composite wing box for flutter and stiffness", In: 48th AIAA Aerospace Sciences Meeting Including the New Horizons Forum and Aerospace Exposition, Orlando: Florida, 2010.

[26] Othman, M. F., Silva, G. H., Cabral, P. H., Prado, A. P., Pirrera, A., & Cooper, J. E., A robust and reliability-based aeroelastic tailoring framework for composite aircraft wings. Composite Structures, 208, 101-113, 2019.

[27] Liu, X., Optimum design of composite structures using lamination parameters (Doctoral dissertation, Cardiff University), 2019.

[28] Farsadi, T., Asadi, D., & Kurtaran, H. "Flutter improvement of a thin walled wing-engine system by applying curvilinear fiber path". Aerospace Science and Technology, 93, 2019, 105353